

Research Article

Investigations on the WEDM of Friction Stir Processed Magnesium/Graphene-Boron Nitride Hybrid Surface Composite through the Entropy-COPRAS Approach

V. Kavimani ¹, P. M. Gopal ¹, V. Sivamaran ², and K. Anand Babu ³

¹Centre for Material Science, Department of Mechanical Engineering, Karpagam Academy of Higher Education, Coimbatore 641021, India

²Department of Mechanical Engineering, Audisankara College of Engineering and Technology (Autonomous), Gudur, India

³Department of Production Engineering, National Institute of Technology, Tiruchirappalli 620015, India

Correspondence should be addressed to V. Kavimani; manikavi03@gmail.com

Received 28 July 2022; Revised 22 September 2022; Accepted 1 October 2022; Published 17 October 2022

Academic Editor: Dhanesh G. Mohan

Copyright © 2022 V. Kavimani et al. This is an open access article distributed under the Creative Commons Attribution License, which permits unrestricted use, distribution, and reproduction in any medium, provided the original work is properly cited.

In this research, friction stir processing (FSP) is utilized to develop the graphene-boron nitride-reinforced hybrid magnesium surface composite with varying volume percentages of reinforcements. A Taguchi-coupled Entropy-COPRAS approach is adopted to understand the influence of control factors of wire electrical discharge machining on the developed magnesium surface composite. An optimal combination of machining factors to attain maximum material removal rate (MRR) along with minimal kerf width and surface roughness is to be finalized. The Taguchi method is utilized for planning the experiments with three levels and four factors, namely, reinforcement volume %, pulse off time, wire feed rate, and pulse on time. ANOVA results show that pulse on time and reinforcement volume % act as the most significant factors for output responses. Using the Entropy-COPRAS approach, an optimal combination for output response was found for a maximum MRR of 16.20 mm³/min; minimal surface roughness of 3.86 μm; and 0.29 μm of kerf width.

1. Introduction

Growing demand for lightweight structural materials in the aerospace and transport industries has resulted in a major interest in magnesium and its alloys. Compared with aluminium and steel, magnesium is one of the engineering materials that weighs the least, which helps with boosted fuel economy and a reduction in pollutants [1, 2]. Likewise, it exhibits a better strength-to-weight ratio, toughness, high damping capacity, and easier machinability. However, these materials have some major limitations, such as low creep, stiffness, low resistance to wear, and increased reactivity towards chemicals that frequently limit their industrial applications. It also has poor ductility, characterized by a brittle-like performance at ambient temperature owing to its HCP crystal structure and a limited slip system [3–5]. Composite development is considered one of the key ways to

enhance the desired strength of Mg matrix material by the addition of selected reinforcements. The inclusion of carbide and carbon-based reinforcement such as SiC, TiC, CNT, graphene, etc. in the magnesium matrix enhances the mechanical characteristics and functional properties [6, 7]. In several industrial applications, material life is mainly dependent on surface mechanical qualities, and hence the development of surface composites has been adopted by several researchers.

Friction stir processing is a surface modification technique used to develop surface composites at a temperature below the substrate's melting point, and there is little literature available based on Mg FSP [8]. Qiao et al. adopted FSP with different passes to develop a ZrO₂-reinforced magnesium surface composite [9]. Investigation over mechanical behaviour depicts improved tensile strength (~15.9%) while compared with base material. Likewise,

increases in FSP pass decrease its grain size. An SiC-reinforced Mg surface composite was developed by Lu et al. through the FSP approach, and optimization was done for the FSP parameters to attain better mechanical properties [10]. Results revealed that FSP of three passes showcases better tensile and hardness properties. A graphene-reinforced Mg surface composite was developed by Zang et al. and its effects on mechanical properties were analyzed [11]. Observed results show that higher rotation speed and three passes increase the tensile and microhardness of the Mg matrix and also found that the addition of graphene up to 6.43 volume % showcased improved strength compared to the base material. Because composite materials are harder, tougher, and more resistant to wear and fatigue, they are more difficult to machine. Though these composites have better properties, the existence of reinforcement particles in the matrix phase harms the cutting tool life during traditional machining, which results in a deprived surface quality of machined engineering parts. Additionally, the inclusion of reinforcement reduces the tool life of traditional tungsten carbide and high-speed steel tools due to abrasion. As a result of their high hardness, composite materials are challenging to process using traditional techniques, particularly where complex geometry and dimensional accuracy are needed.

These composites are easily processed using nontraditional techniques like abrasive water jet machining. However, they can only be cut in one direction with these techniques. Consequently, WEDM has become a good method for shaping complicated materials made of composites. Herein, material removal takes place by erosion formed by sparks in-between the work samples and wire. Conversely, the formation of an immediate rise in temperature due to sparks and variation in melting point among the matrix and reinforcement will affect the surface of machined components. Another fact is that the presence of reinforcement phase in composite forms limits electrical conductivity, which results in damage due to anisotropic thermal distribution. Furthermore, wire breaking owing to the limited build-up current and variation in hardness of the composite is also a limiting factor to reducing the production rate in WEDM. Hence, there is a need for an hour to optimize the control factors to improve the quality of machined surfaces by maintaining higher material removal. It was found that only minimal studies discussed the WEDM of Mg surface composites. Kavimani et al. examined the consequences of WEDM parameters on graphene magnesium composite, and the results revealed that a surge in pulse on time increases MRR [12]. Further, observation revealed that pulse off time and pulse on time have more domination in influencing control parameters over output response. Vijayabhaskar and Rajmohan et al. developed a nano SiC-reinforced Mg composite and discussed the consequences of WEDM control factors on the developed composite [13]. Reinforcement percentage, pulse off time, voltage, pulse on time, and wire feed rate are chosen as input parameters. The results reveal that an increase in reinforcement percentage decreases the surface finish. Progress in newer soft computing techniques results in the development of different optimization

approaches to attain solutions for complex objectives and uncertain situations. For predicting and attaining optimal machining parameters, researchers adopted various mathematical and statistical techniques such as Taguchi, ANN, GA, PSO, etc. [14, 15]. Additionally, a multiresponse optimization strategy was utilized to address the competing natural responses brought on by material removal rate, surface roughness, kerf taper, etc., which prevented the individually optimized settings from accomplishing their goals [16, 17]. From an industrial viewpoint, the ideal combination is necessary to ensure that the defined reactions are obtained in the best possible balance.

This fact made the researchers adopt hybrid optimization techniques, and a little literature on these techniques is discussed in detail. An analytical hierarchy process coupled genetic algorithm approach was adopted by Kumar et al. to optimize WEDM parameters. Input parameters such as wire tension, spark gap-set voltage, pulse on time, pulse peak current, pulse off time, wire feed rate, and other input parameters are selected and optimized for MRR and roughness [18]. At the optimal combination, 13.79% and 19.16% improvements have been attained while compared with discrete optimal solutions. A PCA-coupled ANN approach was adopted by Phate et al. to understand the WEDM behaviour of the developed composite. The results reveal that integrated form optimization techniques deliver an effective optimal solution. Based on available literature, it can be noted that wire feed rate, pulse off time, and pulse on time are the major influencing parameters in WEDM [19]. Machinability analysis of graphene-based surface composites has rarely been reported. Multiobjective optimization techniques deliver better results when compared with traditional techniques. Utilization of Entropy-coupled CORPUS for WEDM analysis is not yet reported. On the basis of the obtained evidence, an attempt has been made to understand the machinability characteristics of graphene-reinforced surface composite. The Entropy-coupled CORPUS methodology is adopted to understand and optimize the machining parameters to improve the quality of the machined surface and production rate in a single unique solution.

2. Materials and Methods

AZ31 Mg alloy substrate with dimensions of $150 \times 100 \times 8$ mm is selected as the base material. Graphene and boron nitride particles are selected as reinforcements to improve the basic and functional properties of the AZ31 Mg alloy. Herein, graphene and boron nitride particles are mixed in equal proportion by the assistance of an ultrasonic assisted stirring process. Herein, the calculated amount of graphene and BN particles are ultrasonicated separately with organic solvent for 1 h, and then the samples are further sonicated for 3 h. After that, the samples are stirred using a magnetic stir coupled with a hot plate for 3 h at 1000 rpm. Then the attained mixtures are vacuum dried for 24 h and the resultant samples are used as reinforcement. The profile of the FSP tool used and the step-by-step procedure for FSP are illustrated in Figures 1(a) and 1(b). As a first step in FSP,

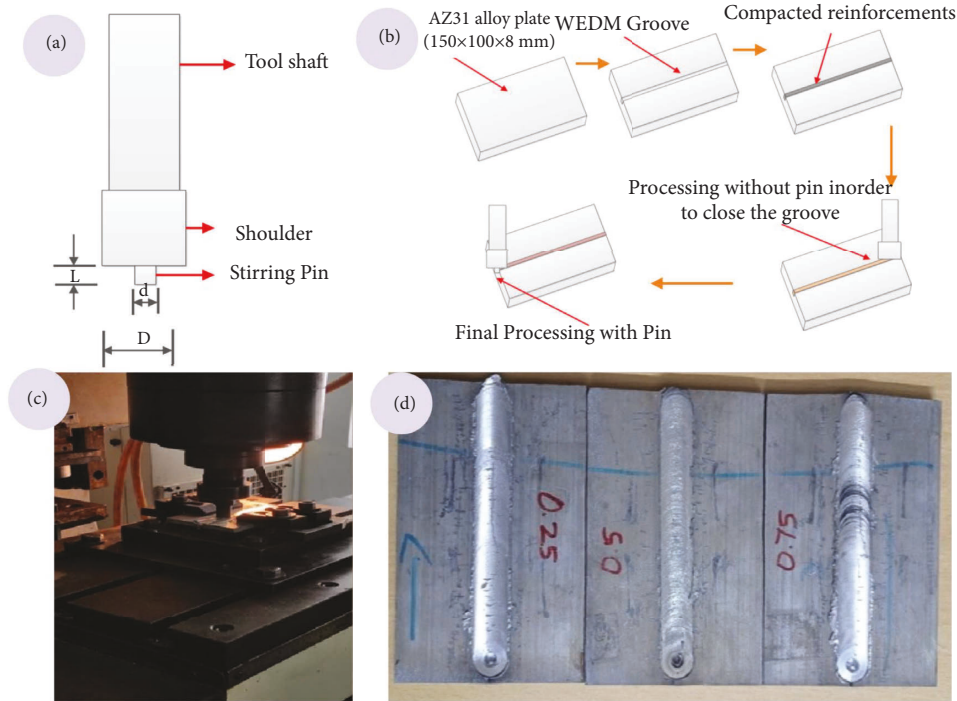


FIGURE 1: (a) Dimension of tool profile. (b) Schematic sketch of FSP. (c) Modified milling machine for the FSP approach. (d) Developed surface composite.

a groove has been made at the center of the Mg plate parallel to its longest side, as shown in Figure 1(b) using the WEDM process. The groove depth is fixed at 5 mm and its width is varied based on volume % of reinforcement (1, 3, and 5). A double-tempered H13 steel tool with a 5 mm pin length (L), a 20 mm diameter shoulder (D), and a 6 mm diameter pin (d) was utilized for FSP. Friction stir processing was conducted in a modified vertical milling machine with an optimized rotation speed and traverse feed of 1200 rpm and 20 mm/min (Figure 1(c)). Initially, the reinforcement mixture is filled in the groove gap and the pin-less tool is allowed to pass for compacting, followed by the passing of the pin-headed tool [20]. The developed surface composite is shown in Figure 1(d).

3. Experimental Design

The Taguchi approach was adopted for the experimental plan with three levels and four factors with the L27 orthogonal array. Based on available literature, pulse off time, pulse on time, and wire feed rate are found to be the most important control factors in WEDM and hence they are chosen as input parameters (Table 1). Similarly, the production rate of a material and the surface quality of mechanical components are mainly based on MRR, surface roughness, and kerf width, respectively, and so these parameters are chosen as output responses (Table 2). Herein, procedures for MRR, surface roughness, and kerf width measurement are already shown in our previous reports [20, 21]. While larger is better condition, it is designated for MRR and smaller is better condition, it is designated for kerf width (KW) and surface roughness during SN ratio analysis,

TABLE 1: Machining parameters and respective levels.

Parameters	Notation	Unit	Level 1	Level 2	Level 3
Reinforcement %	A	Wt. %	1	3	5
Pulse off time	B	Ms	4	8	12
Pulse on time	C	Ms	10	15	20
Wire feed rate	D	m/min	4	6	8

since higher surface roughness (R_a) decreases the surface quality.

4. Results and Discussion

To determine the correlation among the set of variable pairings, a scatter-plot matrix is utilized (Figure 2). It is possible to arrange these pairwise correlations into a matrix. In general, the diagonal arrangement of the current matrix pair shows a stronger correlation between the matrix pairs and a lack of outliers in the obtained output data. Further relations between the various control factors and their respective output responses can also be understood with the help of a matrix plot. It can also be used to observe the clustering of data by control factors in the dataset for a specific response variable. Herein, the correlation set of variables can be identified based on the mirror images. For example, the eighth row fifth column and the ninth row sixth column of the scatter plot resemble the mirror image of the fifth row eighth column and the sixth row ninth column of the scatter plot, which denotes the correlation among data sets. Likewise, the influence of each control factor over other output responses can also be examined using a scatter plot. For example, the fifth column in the first row implies the

TABLE 2: Experimental trails along with output response.

Reinforcement (%)	Pulse off time (μs)	Pulse on time (μs)	Wire feed rate (m/min)	MRR (mm^3/min)	Ra (μm)	KW (μm)
1	4	10	4	12.0765	3.6730	0.2877
1	4	15	6	14.8180	3.7540	0.2905
1	4	20	8	16.2010	3.8610	0.2967
1	8	10	6	12.3505	3.6830	0.2972
1	8	15	8	14.6605	3.7270	0.3027
1	8	20	4	13.4580	3.7630	0.3010
1	12	10	8	11.8400	3.6540	0.3049
1	12	15	4	11.5170	3.6980	0.3053
1	12	20	6	13.3415	3.7670	0.3093
3	4	10	4	10.0170	3.7280	0.2870
3	4	15	6	13.7505	3.8130	0.2948
3	4	20	8	14.8505	3.8960	0.2963
3	8	10	6	10.9015	3.6820	0.2967
3	8	15	8	12.8680	3.7680	0.3014
3	8	20	4	12.2725	3.7750	0.3004
3	12	10	8	11.3505	3.7280	0.3023
3	12	15	4	11.1015	3.7220	0.3032
3	12	20	6	13.1340	3.7960	0.3079
5	4	10	4	9.2265	3.7260	0.2873
5	4	15	6	12.6765	3.8290	0.2897
5	4	20	8	13.9850	3.8820	0.2916
5	8	10	6	9.9400	3.7430	0.2930
5	8	15	8	13.2080	3.8110	0.2947
5	8	20	4	11.3830	3.8230	0.2969
5	12	10	8	10.0180	3.7480	0.2972
5	12	15	4	9.6890	3.7590	0.3002
5	12	20	6	10.9415	3.8250	0.3010

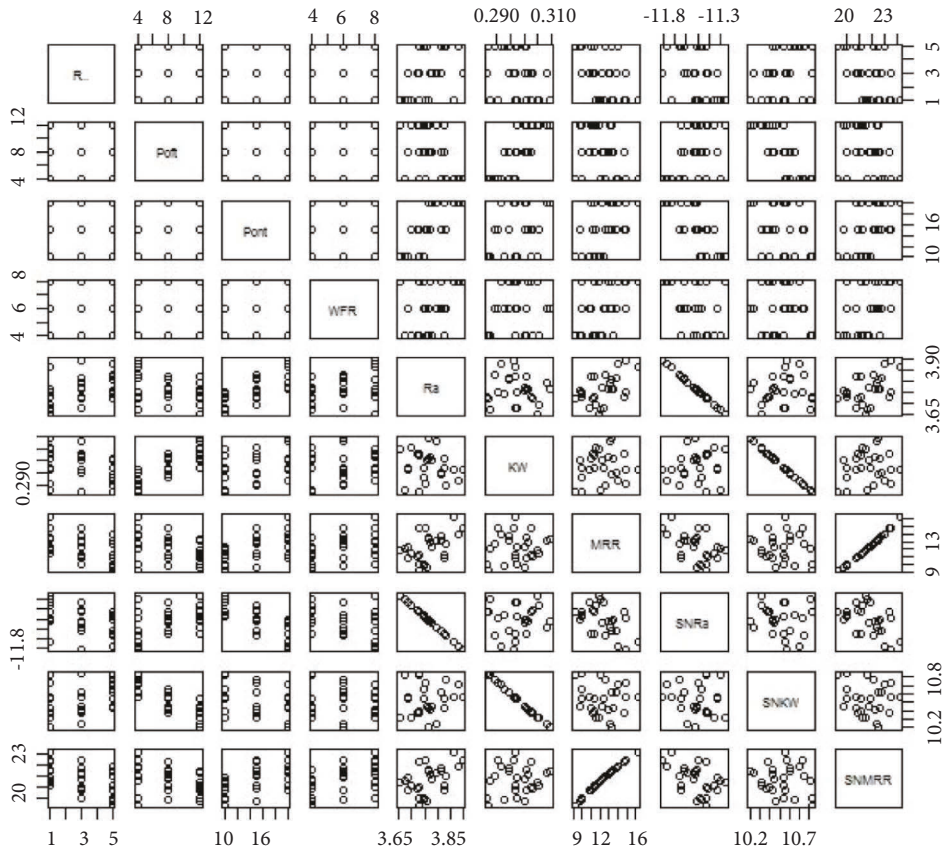


FIGURE 2: Matrix scatter plot of the L27 OA dataset.

relation between surface roughness and reinforcement percentage. In this, the x -axis denotes the surface roughness, and the y -axis denotes the reinforcement percentage. The movement of variables from left to right indicates that surface roughness increases with respect to reinforcement increment.

An algorithmic analysis known as a “hierarchical cluster” groups the related data into clusters. Each cluster, in this case, differs from the others, and the values are very close to one another. Figure 3 shows that the output parameter values are clustered into four groups using the expressive colours of blue and brown (dark and lighter). According to the input parameter, these are ranked from -1 to 1 . The output parameter values are presented in lighter and darker shades of blue and brown in a top-to-bottom arrangement.

4.1. Effect of Control Factors on Surface Roughness. In Figure 4 depicts the influence of control factors on surface quality. It can be noted that increases in reinforcement decrease the surface roughness as the presence of reinforcement particles promotes the hardness values of the developed composite that results in breakage of wires during the WEDM process, thus decreasing the surface finish. The thermal mismatch between the matrix and reinforcement also plays a vital role in surface roughness. During pulse on time, the creation of sparks results in the melting of base material due to its low melting point. Compared with reinforcement (Graphene: BN), further gets flushed out by the dielectric medium at pulse off time. These reinforcement particles do not melt and stick to the matrix, increasing its surface roughness [12].

Another reason is the presence of BN, which is a well-known wide band gap semiconductor that decreases the chance for the production of sparks and results in improper cuts during machining. It can also be shown that increases in pulse off time increase the surface quality of developed samples. This upsurge in pulse off time results in the absence of spark generation and splashing of dielectric fluid. This fact removes the burs and debris formed over the machined surface. Thus, surface quality increases. Likewise, an increase in the pulse on time upsurges surface roughness that might be owing to the effect of spark generation that creates harder heat affected zones near the machined surface, thus increasing the surface roughness [22]. A rise in wire feed rate decreases the surface quality since the surge in wire feed rate results in newer wire recovery at a faster phase during the machining process. This fact increases the quality and efficiency of generated sparks that form deeper craters over the machined surface, thus reducing the surface finish. Among the available control factors, pulse on time acts as the key parameter in governing the surface quality of the developed composite, followed by reinforcement percentage in second position (Table 3). Wire feed rate has low significance on surface finish [23].

Further, the contribution percentage of individual parameters and their significance can be confirmed by the ANOVA results shown in Table 4. In general, P values of control factor less than 0.05 are deliberated as significant parameters.

It can be observed from Table 4 that all the P values are less than 0.05 , which implies that selected parameters have an influence over the surface quality of the developed composite. The individual contributions of machining parameters are shown in Table 4, that indicates that pulse on time has the major contribution of 58.53% followed by reinforcement volume percentage with a contribution percentage of 18.18% . Herein, wire feed rate delivers a lower contribution of 9.3% . Furthermore, the attained results well coincide with the output response table. The obtained ANOVA results showcase an R square value of 93.2% significance. A mathematical model was developed based on the attained values to predict the surface roughness (equation (1)) of the developed sample with an R square value of 93.41% . The variation in experimental and predicate values is implied in Figure 5.

$$\begin{aligned} \text{SR} = & 3.53036 + 0.0157444 \text{ reinforcement\%} \\ & -0.00645972 \text{ pulse off} + 0.0113478 \\ & \text{pulse on} + 0.0113222 \text{ wire feed.} \end{aligned} \quad (1)$$

The optimal parameters can be attained from the response table. It states that lower values of wire feed rate, pulse on time, and reinforcement volume % with a higher value of pulse off time are optimal solutions for higher surface quality.

4.2. Influence of Control Factors on Kerf Width. Figure 6 infers the impact of control factors on kerf width in the WEDM slot on the developed composite. It can be observed that increases in reinforcement percentage decrease the kerf width of the samples. The addition of reinforcement improves the hardness, which decreases the chances of widening of the sample during the machining process. Further, graphene and BN have better thermal stability that decreases the intensity and heat dissipation over the composite at spark generation, thus decreasing the kerf width. Increment in pulse on time increases the kerf width as more pulse on time maximises the discharge current or energy over the electrode that results in more dielectric supply which causes material evaporation. Likewise, higher pulse on time improves the transfer dissipation inside near the workpiece and dielectric fluid, thus increasing the kerf width. This fact initiates confined heat over the material that erodes a large portion of the material and causes widening of the kerf and profounder craters. During machining, an increase in pulse off time increases flushing time that results in debris and burs over the machined surface that results in a higher kerf width. Lower pulse off time causes inadequate flushing time, which results in the creation of a recast layer over the surface of the machined component that decreases the kerf width. Herein, lower kerf width can be obtained during minimal energy discharge that improvises exactness in dimension [13]. Likewise, an increase in wire feed rate increases kerf width; this might be due to an increase in the intensity of generated sparks. Another reason is increment in wire feed rate increases wire tension and vibration of the wire that causes irregular cuttings on the machined surface [24].

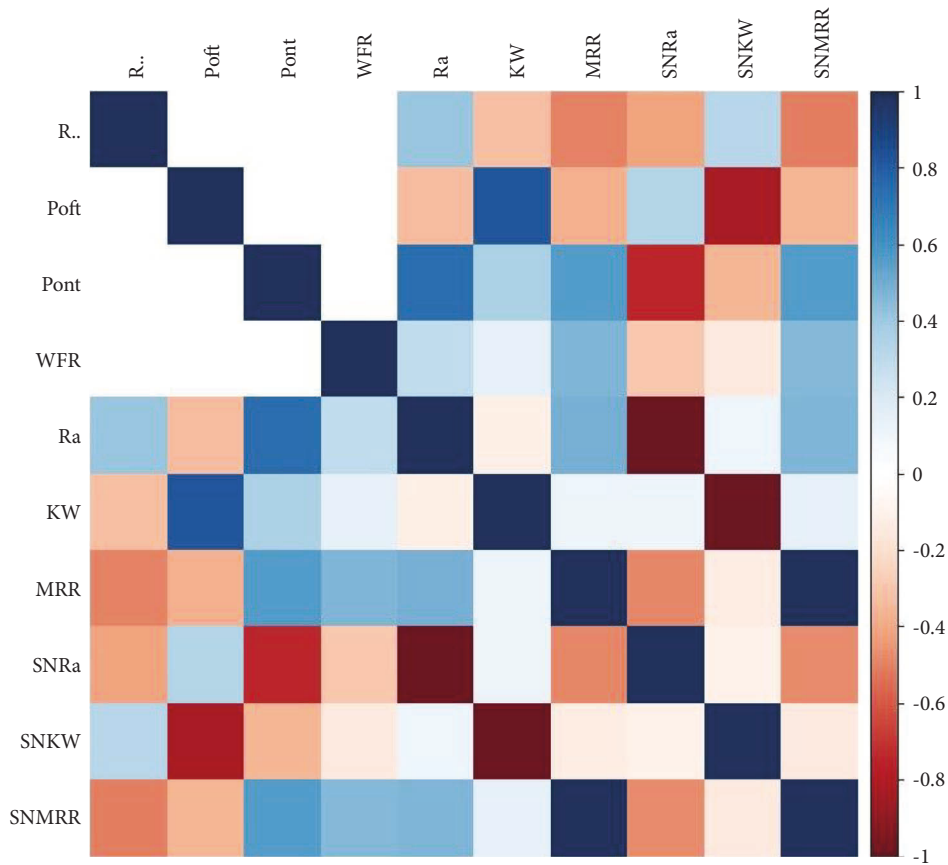


FIGURE 3: Hierarchical clustering of the correlation coefficient matrix of input variables.

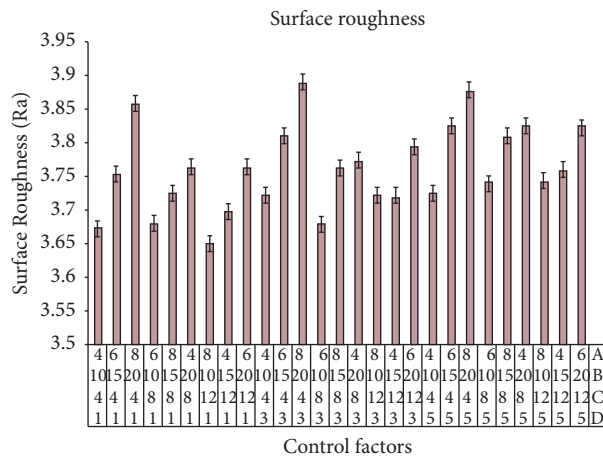


FIGURE 4: Effect of control factors on surface roughness.

TABLE 3: Response table for surface roughness.

Level	Reinforcement %	Pulse off time	Pulse on time	Wire feed rate
1	-11.44	-11.58	-11.38	-11.46
2	-11.52	-11.49	-11.51	-11.52
3	-11.58	-11.47	-11.64	-11.56
Delta	0.15	0.12	0.26	0.1
Rank	2	3	1	4

TABLE 4: ANOVA table for surface roughness.

Source	DF	Seq. SS	Adj. SS	MS	F	P	Contribution (%)
Reinforcement vol.%	2	0.017996	0.017996	0.008998	33.1	0	17.32
Pulse off time	2	0.013792	0.013792	0.006896	25.37	0	13.28
Pulse on time	2	0.057949	0.057949	0.028974	106.59	0	55.78
Wire feed rate	2	0.009264	0.009264	0.004632	17.04	0	8.92
Error	18	0.004893	0.004893	0.000272			
Total	26	0.103893					

R-square=93.20%

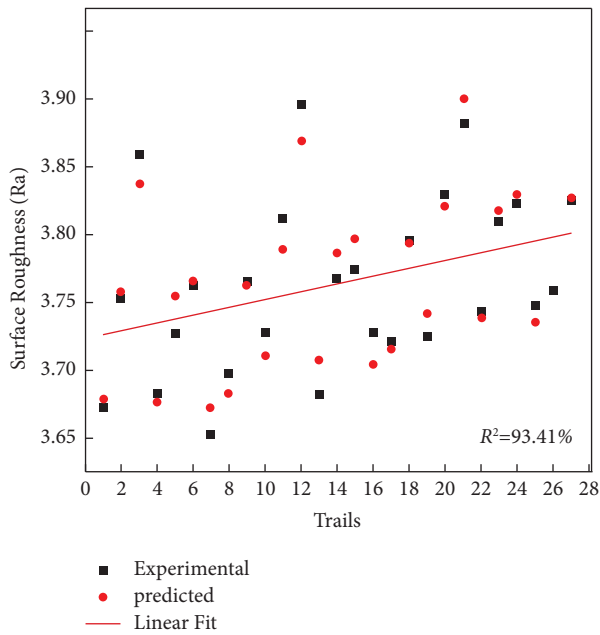


FIGURE 5: Variation between experimental and predicted values of surface roughness.

The response table revealed that pulse off time acts as more dominating parameter in governing kerf width (Table 5), followed by pulse on time. Herein, wire feed rate depicts lower influence over kerf width. From the response table, it can be noted that an increasing percentage of reinforcement and minimal values of control factors is the optimal parameter combination. $10\ \mu\text{s}$ of pulse on time with a pulse off time of $4\ \mu\text{s}$ and a $4\ \text{m/mm}$ of wire feed rate is the optimal solution for obtaining a lower kerf width. From Table 6, it can be inferred that P value is lower than that of 0.05 for every control parameter, which depict that all the machining parameters has significant effect over the output response. The contributions of individual parameters are computed by dividing the sequential sum of square values of each parameter by total sequential sum of square values. The attained values are illustrated in Table 6. The obtained results have a 95.3% significant confidence level. As shown early in the response table, pulse off time has a higher contribution percentage of 70.9% followed by pulse on time and reinforcement volume % that contribute more or less equal percentages of 13.6 & 13.3%, respectively. As inferred from ANOVA results, wire feed rate acts as the lower significant

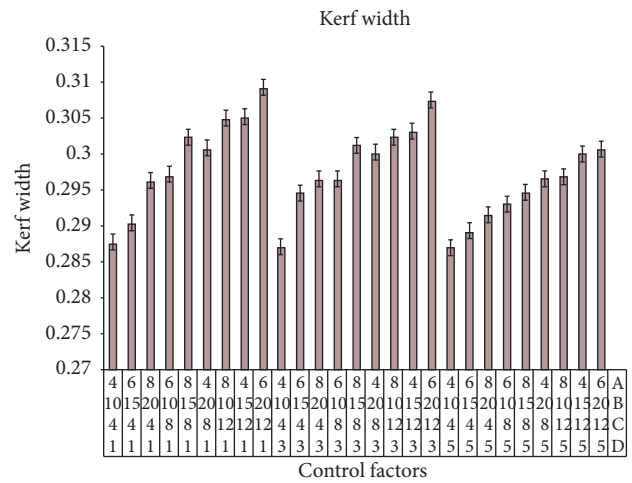


FIGURE 6: Effect of machining parameters on kerf width.

TABLE 5: Response table for kerf width.

Levels	Reinforcement %	Pulse off time	Pulse on time	Wire feed rate
1	10.47	10.71	10.61	10.56
2	10.49	10.51	10.52	10.52
3	10.62	10.36	10.46	10.5
Delta	0.14	0.36	0.16	0.06
Rank	3	1	2	4

parameter with a 2.09% contribution. A mathematical model has been developed to predict the kerf width as illustrated in equation (2). The variation in experimental and predicted values is shown in Figure 7.

$$\begin{aligned} \text{Kerf width} = & 0.278016 - 0.00121389 \text{ reinforcement \%} \\ & + 0.00152361 \text{ pulse off time} \\ & + 0.000531111 \text{ pulse on time} \\ & + 0.000522222 \text{ wire feed rate.} \end{aligned} \tag{2}$$

4.3. Effect of Control Factors on MRR. Figure 8 shows the consequence of control factors on the rate of material removal. It can be observed from the figure that an increase in volume % of reinforcement decreases MRR values. This might be due to the presence of graphene and BN particles that decrease the intensity of spark generation, so the machining rate decreases. Further, these particles have varying electrical conductivity when

TABLE 6: ANOVA table for kerf width.

Source	DF	Seq. SS	Adj. SS	MS	F	P	Contribution (%)
Reinforcement	2	0.0001264	0.0001264	6.32E-05	24.81	0	12.72
Pulse off time	2	0.0006728	0.0006728	0.000336	132.06	0	67.69
Pulse on time	2	0.000129	0.000129	6.45E-05	25.32	0	12.98
Wire feed rate	2	0.0000198	0.0000198	9.9E-06	3.9	0.039	1.99
Error	18	0.0000459	0.0000459	0.0000025			
Total	26	0.0009939					

$R^2 = 95.39\%$

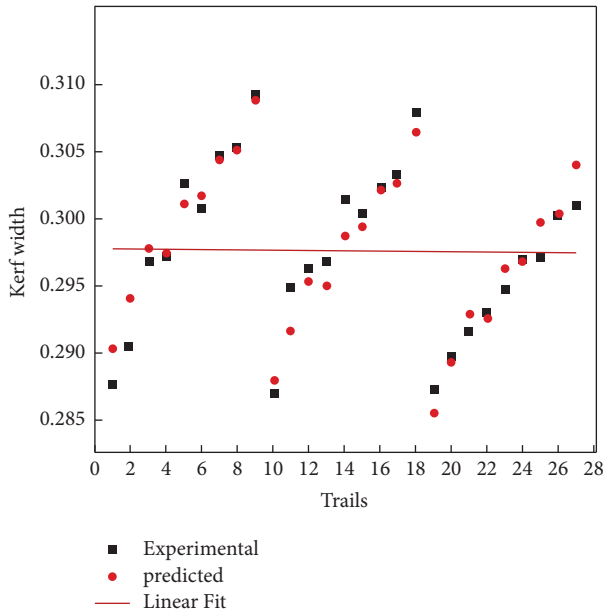


FIGURE 7: Variation between experimental and predicted values of Kerf width.

compared with the base matrix material, which thus decreases the generation of sparks. The hybrid reinforcement has higher thermal stability. This fact decreases the chances of melting of composite material, which increases the machining time. Similarly, an increment in pulse off time decreases MRR values. During pulse off time, the machining process will be in idle condition and no spark generation will happen, which decreases the production rate. An increase in pulse on time increases the MRR value since an increase in the pulse on time promotes the spark cohort time that increases the MRR. It could be shown that increases in wire feed rate increase MRR [12, 23]. During machining conditions, increases in the wire feed rate increase the chance of changeover on new wires that increase the intensity of the spark generated near the work piece, which results in higher MRR. The response table shows that pulse on time is the key dominant parameter for governing the MRR, and pulse off time attains the last position in influencing the MRR. From the response table, the optimal solution for MRR can be attained. Herein, higher values of pulse on time and wire feed followed by lower addition of reinforcement and pulse off time is the optimal condition for a better production rate (Table 7).

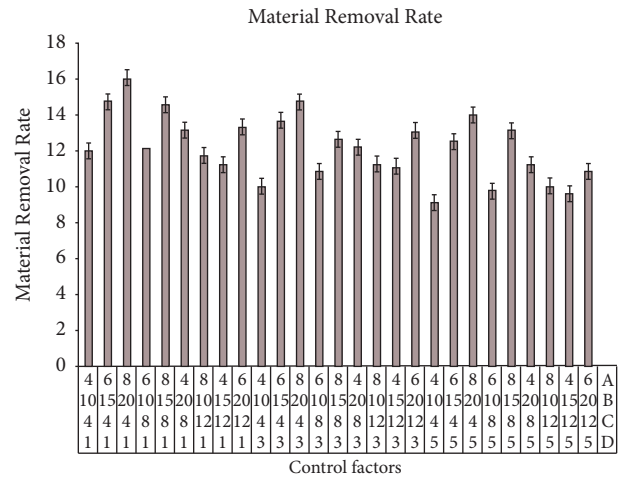


FIGURE 8: Influence of machining parameters on MRR.

TABLE 7: Response table for MRR.

Levels	Reinforcement (%)	Pulse off time	Pulse on time	Wire feed rate
1	22.46	22.19	20.67	20.92
2	21.7	21.77	22	21.83
3	20.92	21.12	22.41	22.34
Delta	1.54	1.07	1.73	1.42
Rank	2	4	1	3

The significance of machining parameters and their respective contributions are inferred from ANOVA (Table 8). Based on ANOVA results, P value < 0.05 indicated that all the control parameters have an influence over the output response. It can be illustrated from Table 8 that pulse on time has more contribution (36.03%) in dominating the output response followed by reinforcement volume % and wire feed rate with more or less equal contribution over materials removal rate. Herein, pulse off time showcases a minimal contribution of 14.9% in governing the output response. An empirical model has been established by the linear regression method to foresee the MRR of a composite as shown in equation (3). The developed model has better predictability with an R square value of 93.18%, as shown in Figure 9.

TABLE 8: ANOVA for MRR.

Source	DF	Seq. SS	Adj. SS	MS	F	P	Contribution (%)
Reinforcement %	2	20.483	20.483	10.242	62.41	0	24.65
Pulse off time	2	11.998	11.998	5.999	36.56	0	14.44
Pulse on time	2	28.876	28.876	14.438	87.98	0	34.75
Wire feed rate	2	18.778	18.778	9.389	57.22	0	22.60
Error	18	2.954	2.954	0.164			
Total	26	83.089					

$R^2 = 96.45\%$

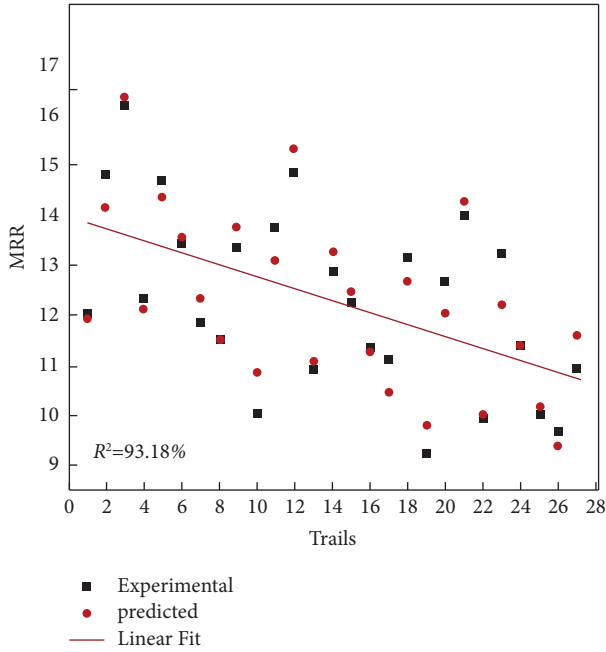


FIGURE 9: Experimental versus predicted values of MRR.

$$\begin{aligned}
 \text{MRR} = & 8.8289 - 0.533208 * \text{reinforcement \%} \\
 & - 0.203729 * \text{pulse off time} \\
 & + 0.242739 * \text{pulse on time} \\
 & + 0.506681 * \text{wire feed rate.}
 \end{aligned} \quad (3)$$

4.4. Multiresponse Optimization of Control Factors. Mutual optimal parameter combinations for two or more output parameters can be obtained with the assistance of multiobjective optimization. The determination of an accurate weight for the output response is the foremost difficulty in multiresponse optimization. Researchers determined the weightage for the response based on their familiarity with and trial and error method related to the control factors' significance [25]. Hence, there is a need to develop a new approach for computing the weightage for the output response. In this proposed research, the entropy method was adopted for allotting individual weightage on output response, which was earlier used for several multicriteria decision making problems. Most of the time, the decision maker expresses their ideas by taking into account choice variables in order to determine the weights for their

traits and to parallelize comparisons with actual-world circumstances. Since entropy weight is a quantity that represents a criterion's relevance in terms of the relative weights of criteria, the entropy method does not require such a choice. When more factors are taken into account, the entropy idea might be used to reduce the human errors involved in assigning weights. The steps involved in the entropy approach are illustrated as follows [26]:

Step 1: normalization of decision matrix EI:

$$E_{ij} = \frac{K_{ij}}{\sum_{i=1}^p K_{ij}}, \quad (4)$$

$$E_{ij} = \frac{1/K_{ij}}{\sum_{i=1}^p 1/K_{ij}}. \quad (5)$$

Herein, (4) is used for maximization function, and (5) is used for normalizing the minimization function (refer to Table 9)

Step 2: calculation of entropy index:

$$I_e = - \left[\frac{\sum_{i=1}^l E_{ij} \ln(E_{ij})}{\ln(l)} \right]. \quad (6)$$

Entropy index of the normalized values can be obtained from equation (6). The calculated values are illustrated in Table 10.

Step 3: determination of weightage:

$$W_e = \frac{1 - I_e}{\sum_{e=1}^n (1 - I_e)}. \quad (7)$$

The values attained for individual parameters from (7) can be used as weightage for the hybrid optimization approaches as shown in Table 10. In this research, entropy-coupled Complex Proportional Assessment (COPRAS) was adopted to attain an optimal solution for better MRR with better surface quality.

4.5. Multiobjective Optimization by the Entropy-Coupled Complex Proportional Assessment Approach. The COPRAS approach involves proportional and direct confidence in the significance and effectiveness of substitutions available in the existence of equally conflicting parameters [27]. COPRAS incorporates the success of alternatives in relation to several control factors and connects the weights by ranking and suggesting the optimal parameters. The

TABLE 9: Entropy modelling for output variables.

Maximize function	Minimization function		Normalization			Entropy index (EI)		
	MRR	Ra	KW	MRR	Ra	KW	EIMRR	EIRa
12.0765	3.673	0.2877	0.0364	0.0027	0.0383	-0.1206	-0.0159	-0.1250
14.818	3.754	0.2905	0.0447	0.0026	0.0379	-0.1389	-0.0156	-0.1241
16.201	3.861	0.2967	0.0489	0.0025	0.0371	-0.1475	-0.0152	-0.1223
12.3505	3.683	0.2972	0.0372	0.0027	0.0371	-0.1226	-0.0158	-0.1222
14.6605	3.727	0.3027	0.0442	0.0026	0.0364	-0.1379	-0.0157	-0.1206
13.458	3.763	0.3010	0.0406	0.0026	0.0366	-0.1301	-0.0155	-0.1211
11.84	3.654	0.3049	0.0357	0.0027	0.0361	-0.1190	-0.0159	-0.1200
11.517	3.698	0.3053	0.0347	0.0027	0.0361	-0.1167	-0.0158	-0.1199
13.3415	3.767	0.3093	0.0402	0.0026	0.0356	-0.1293	-0.0155	-0.1188
10.017	3.728	0.2870	0.0302	0.0026	0.0384	-0.1057	-0.0157	-0.1252
13.7505	3.813	0.2948	0.0415	0.0026	0.0374	-0.1320	-0.0154	-0.1229
14.8505	3.896	0.2963	0.0448	0.0025	0.0372	-0.1391	-0.0151	-0.1224
10.9015	3.682	0.2967	0.0329	0.0027	0.0371	-0.1123	-0.0158	-0.1223
12.868	3.768	0.3014	0.0388	0.0026	0.0366	-0.1261	-0.0155	-0.1210
12.2725	3.775	0.3004	0.0370	0.0026	0.0367	-0.1220	-0.0155	-0.1213
11.3505	3.728	0.3023	0.0342	0.0026	0.0365	-0.1155	-0.0157	-0.1207
11.1015	3.722	0.3032	0.0335	0.0026	0.0363	-0.1137	-0.0157	-0.1205
13.134	3.796	0.3079	0.0396	0.0026	0.0358	-0.1279	-0.0154	-0.1192
9.2265	3.726	0.2873	0.0278	0.0026	0.0384	-0.0997	-0.0157	-0.1251
12.6765	3.829	0.2897	0.0382	0.0026	0.0380	-0.1248	-0.0153	-0.1244
13.985	3.882	0.2916	0.0422	0.0025	0.0378	-0.1335	-0.0152	-0.1238
9.94	3.743	0.293	0.0300	0.0026	0.0376	-0.1051	-0.0156	-0.1234
13.208	3.811	0.2947	0.0398	0.0026	0.0374	-0.1284	-0.0154	-0.1229
11.383	3.823	0.2969	0.0343	0.0026	0.0371	-0.1158	-0.0153	-0.1223
10.018	3.748	0.2972	0.0302	0.0026	0.0371	-0.1057	-0.0156	-0.1222
9.689	3.759	0.3002	0.0292	0.0026	0.0367	-0.1032	-0.0156	-0.1213
10.9415	3.825	0.301	0.0330	0.0026	0.0366	-0.1126	-0.0153	-0.1211

TABLE 10: Calculated weighted entropy values.

Degree of divergence			Entropy weights		
MRR	Ra	Kw	MRR	Ra	Kw
0.0031	0.8726	0.0001	0.00352832	0.99639944	0.00007224

following steps are involved in the COPRAS approach as follows [28]:

Step 1: The initial step involves formation of decision matrix followed by normalization of output parameter.

$$NOij = \frac{Qij}{\sqrt{\sum_{i=1}^m Qij^2}} \tag{8}$$

Step 2: This involves multiplication of calculated individual weight to create a normalized decision matrix. Herein, weightage calculated from the entropy approach will be multiplied with a normalized matrix (equation (9)) to form a weighted matrix as shown in Table 9.

$$NWij = We X NOij. \tag{9}$$

Step 3: calculation of Pi

In this, Pi is maximization function calculated by

$$Pi = \sum_{j=1}^n Qij. \tag{10}$$

Here, n is number of maximizing response.

Step 4: calculation of Ri.

In this Ri, denote the minimization function calculated by

$$Ri = \sum_{j=m+1}^n Qij. \tag{11}$$

The calculated values are summarized, and the calculated values are illustrated in Table 11.

Step 5: Observing the diminutive value of R.

$$Rmin = \min Ri. \tag{12}$$

Step 6: Determination of weight for attained individual response Qi

The Qi values are calculated by using equation (13), and the maximum value in Qi is termed as Qmax.

$$Qi = Pi + \frac{Rmin \sum_{j=1}^m Ri}{Ri \sum_{j=1}^m Rmin/Ri} \tag{13}$$

TABLE 11: Computed attributes values.

Weighted normalized matrix			Pi	Ri
MRR	Ra	KW	MRR	Ri
0.00012851	0.03600936	0.00000259	0.00012851	0.03601194
0.00015768	0.03680347	0.00000261	0.00015768	0.03680608
0.00017240	0.03785247	0.00000267	0.00017240	0.03785514
0.00013142	0.03610740	0.00000267	0.00013142	0.03611007
0.00015600	0.03653876	0.00000272	0.00015600	0.03654148
0.00014321	0.03689170	0.00000271	0.00014321	0.03689441
0.00012599	0.03582309	0.00000274	0.00012599	0.03582583
0.00012255	0.03625445	0.00000274	0.00012255	0.03625720
0.00014197	0.03693092	0.00000278	0.00014197	0.03693370
0.00010659	0.03654857	0.00000258	0.00010659	0.03655115
0.00014632	0.03738189	0.00000265	0.00014632	0.03738454
0.00015802	0.03819561	0.00000266	0.00015802	0.03819827
0.00011600	0.03609759	0.00000267	0.00011600	0.03610026
0.00013693	0.03694072	0.00000271	0.00013693	0.03694343
0.00013059	0.03700935	0.00000270	0.00013059	0.03701205
0.00012078	0.03654857	0.00000272	0.00012078	0.03655128
0.00011813	0.03648974	0.00000273	0.00011813	0.03649247
0.00013976	0.03721523	0.00000277	0.00013976	0.03721799
0.00009818	0.03652896	0.00000258	0.00009818	0.03653154
0.00013489	0.03753875	0.00000260	0.00013489	0.03754136
0.00014882	0.03805835	0.00000262	0.00014882	0.03806097
0.00010577	0.03669562	0.00000263	0.00010577	0.03669826
0.00014055	0.03736228	0.00000265	0.00014055	0.03736493
0.00012113	0.03747993	0.00000267	0.00012113	0.03748260
0.00010660	0.03674464	0.00000267	0.00010660	0.03674731
0.00010310	0.03685249	0.00000270	0.00010310	0.03685518
0.00011643	0.03749954	0.00000271	0.00011643	0.03750224

TABLE 12: Optimal criteria and ranking.

Rimin/Ri	Qi	Ni (%)	Ranking
0.994832	0.001497	92.92797	23
0.973367	0.001557	96.61189	7
0.946393	0.001611	100	1
0.992128	0.001504	93.3404	19
0.980415	0.001545	95.8837	12
0.971037	0.001546	95.92208	11
1	0.001488	92.33272	26
0.988102	0.001501	93.13701	21
0.970004	0.001546	95.93782	10
0.980156	0.001496	92.8398	24
0.958306	0.001567	97.27148	4
0.937891	0.00161	99.91754	2
0.992398	0.001488	92.3603	25
0.969748	0.001541	95.64807	14
0.96795	0.001537	95.41665	15
0.980152	0.00151	93.7208	16
0.981732	0.001505	93.41761	17
0.962594	0.001554	96.47144	8
0.980682	0.001487	92.27149	27
0.954303	0.001562	96.93211	5
0.941275	0.001595	99.02206	3
0.976227	0.001501	93.13598	22
0.958809	0.001561	96.86694	6
0.955799	0.001546	95.93924	9
0.974924	0.001503	93.30322	20
0.97207	0.001504	93.3404	18
0.955298	0.001542	95.694	13

Step 7: Determination of the utility degree N_i %.

$$N_i = 100 \times (Q_i/Q_{\max}). \quad (14)$$

Based on the utility degree, the maximum value is ranked as the optimal parameter and the calculated values are shown in Table 12.

Based on the entropy-coupled corpus method, optimal control factors to attain better MRR along with minimal Ra and kerf width are attained. Herein, lower pulse off time and volume percentage of reinforcement with higher values of wire feed rate and pulse on time are the optimal machining parameters for attaining a good quality machined surface and production rate for the developed composite. The optimal parameter attained based on the hybrid approach (highlighted in bold font) yields the outcome values of 16.20 mm³/min of MRR with 0.29 μm of kerf width and minimal surface roughness of 3.86 μm.

5. Conclusion

A magnesium surface composite with varying volume percentages of hybrid reinforcement was developed by the friction stir processing route. The WEDM process was used to understand the machinability of magnesium surface composites. The Taguchi approach was utilized for planning the experiment. The obtained results are as follows:

- (i) Pulse on time and reinforcement volume percentage act as the dominating factors to influence MRR, kerf width, and surface roughness.
- (ii) Lower values of pulse on time and reinforcement volume %; higher values of wire feed rate and pulse off time are the optimal machining control factors for attaining better surface integrity
- (iii) Wire feed rate has the least significance over output responses.
- (iv) Entropy-coupled COPRAS was adopted to attain an optimal solution, viz. a wire feed rate of 8 m/min, 1 volume % of reinforcement, 20 μs of pulse on time, and 4 μs of pulse off time.
- (v) mathematical model has been developed based on the correlation between the output and input parameters with better predictability.
- (vi) In the future, artificial neural networks can be used to develop models for composite machining and to predict the output response without wasting the work sample with various experimental trials.
- (viii) The developed composite can be used in potential industrial applications where lightweight structures with high hardness and wear-resisting surfaces are needed.

Data Availability

The raw/processed data required to reproduce these findings cannot be shared at this time as the data also form part of an ongoing study.

Conflicts of Interest

The authors declare that they have no conflicts of interest.

References

- [1] S. Banerjee, S. Poria, G. Sutradhar, and P. Sahoo, "Dry sliding tribological behavior of AZ31-WC nano-composites," *J Magnes Alloy*, vol. 7, pp. 315–327, 2019.
- [2] S. Zhang, X. Ma, R. Wu, Q. Ji, F. Zhong, and X. Wang, "Effect of Sn alloying and cold rolling on microstructure and mechanical properties of Mg[Sn]14Li alloy," *Materials Characterization*, vol. 182, Article ID 111491, 2021.
- [3] M. Y. Zhou, L. B. Ren, L. L. Fan, Y. W. X. Zhang, T. H. Lu, and G. F. Quan, "Progress in research on hybrid metal matrix composites," *Journal of Alloys and Compounds*, vol. 838, 2020.
- [4] F. Guo, L. Liu, Y. Ma, L. Jiang, D. Zhang, and F. Pan, "Mechanism of phase refinement and its effect on mechanical properties of a severely deformed dual-phase Mg–Li alloy during annealing," *Materials Science and Engineering A*, vol. 772, Article ID 138792, 2020.
- [5] M. S. Jalali, A. Zarei-Hanzaki, M. Mosayebi, H. R. Abedi, M. Malekan, and M. Kahnooji, "Unveiling the influence of dendrite characteristics on the slip/twinning activity and the strain hardening capacity of Mg–Sn–Li–Zn cast alloys," *J Magnes Alloy*, 2022.
- [6] K. Dharmalingam, G. Padmavathi, A. B. Kunnumakkara, and R. Anandalakshmi, "Microwave-assisted synthesis of cellulose/zinc-sulfate-calcium-phosphate (ZSCAP) nano-composites for biomedical applications," *Materials Science and Engineering: C*, vol. 100, pp. 535–543, 2019.
- [7] V. Kavimani, K. S. Prakash, M. S. Starvin, B. Kalidas, V. Viswamithran, and S. R. Arun, "Tribosurface characteristics and wear behaviour of SiC@r-GO/Mg composite worn under varying control factor," *Silicon*, vol. 12, no. 1, pp. 29–39, 2020.
- [8] Q. Liu, Q. x Ma, G. q Chen et al., "Enhanced corrosion resistance of AZ91 magnesium alloy through refinement and homogenization of surface microstructure by friction stir processing," *Corrosion Science*, vol. 138, pp. 284–296, 2018.
- [9] K. Qiao, T. Zhang, K. Wang et al., "Effect of multi-pass friction stir processing on the microstructure evolution and corrosion behavior of ZrO₂/AZ31 magnesium matrix composite," *Journal of Materials Research and Technology*, vol. 18, pp. 1166–1179, 2022.
- [10] Y. Lu, W. Li, F. Luo et al., "Mechanical properties and corrosion behavior of a friction stir processed magnesium alloy composite AZ31B–SiC," *Materials Testing*, vol. 64, no. 3, pp. 314–322, 2022.
- [11] Q. Zang, H. Chen, J. Zhang, L. Wang, S. Chen, and Y. Jin, "Microstructure, mechanical properties and corrosion resistance of AZ31/GNPs composites prepared by friction stir processing," *Journal of Materials Research and Technology*, vol. 14, pp. 195–201, 2021.
- [12] V. Kavimani, K. S. Prakash, and T. Thankachan, "Influence of machining parameters on wire electrical discharge machining performance of reduced graphene oxide/magnesium composite and its surface integrity characteristics," *Composites Part B: Engineering*, vol. 167, pp. 621–630, 2019.
- [13] S. Vijayabhaskar and T. Rajmohan, "Experimental investigation and optimization of machining parameters in WEDM of nano-SiC particles reinforced magnesium matrix composites," *Silicon*, vol. 11, no. 4, pp. 1701–1716, 2019.

- [14] Y. Al-Dunainawi, M. F. Abbod, and A. Jizany, "A new MIMO ANFIS-PSO based NARMA-L2 controller for nonlinear dynamic systems," *Engineering Applications of Artificial Intelligence*, vol. 62, pp. 265–275, 2017.
- [15] A. C. Y. Yuen, T. B. Y. Chen, C. Wang et al., "Utilising genetic algorithm to optimise pyrolysis kinetics for fire modelling and characterisation of chitosan/graphene oxide polyurethane composites," *Composites Part B: Engineering*, vol. 182, Article ID 107619, 2020.
- [16] V. Kavimani, K. S. Prakash, T. Thankachan, S. Nagaraja, A. K. Jeevanantham, and J. P. Jhon, "WEDM parameter optimization for silicon@r-GO/magnesium composite using taguchi based GRA coupled PCA," *Silicon*, vol. 12, no. 5, pp. 1161–1175, 2020.
- [17] P. M. Gopal, "Wire electric discharge machining of silica rich E-waste CRT and BN reinforced hybrid magnesium MMC," *Silicon*, vol. 11, no. 3, pp. 1429–1440, 2019.
- [18] A. Kumar, N. Grover, A. Manna et al., "Multi-objective optimization of WEDM of aluminum hybrid composites using AHP and genetic algorithm," *Arabian Journal for Science and Engineering*, vol. 47, no. 7, pp. 8031–8043, 2021.
- [19] M. R. Phate, S. B. Toney, and V. R. Phate, "Multi-parametric optimization of WEDM using artificial neural network (ANN)-based PCA for Al/SiCp MMC," *Journal of the Institution of Engineers*, vol. 102, no. 1, pp. 169–181, 2021.
- [20] T. Thankachan, K. Soorya Prakash, and M. Loganathan, "WEDM process parameter optimization of FSPed copper-BN composites," *Materials and Manufacturing Processes*, vol. 33, no. 3, pp. 350–358, 2018.
- [21] R. Gopal, K. Thirunavukkarasu, V. Kavimani, and P. M. Gopal, "Measurement and multi-response optimization of spark erosion machining parameters for titanium alloy using hybrid taguchi-grey relational analysis-principal component analysis approach," *Journal of Materials Engineering and Performance*, vol. 30, no. 4, pp. 3129–3143, 2021.
- [22] K. Mouralova, L. Benes, R. Zahradnicek et al., "Analysis of cut orientation through half-finished product using WEDM," *Materials and Manufacturing Processes*, vol. 34, no. 1, pp. 70–82, 2019.
- [23] V. Kavimani, K. Soorya Prakash, and T. Thankachan, "Multi-objective optimization in WEDM process of graphene – SiC-magnesium composite through hybrid techniques," *Measurement*, vol. 145, pp. 335–349, 2019.
- [24] K. Mouralova, J. Kovar, L. Klakurkova, T. Prokes, and M. Horynova, "Comparison of morphology and topography of surfaces of WEDM machined structural materials," *Measurement*, vol. 104, pp. 12–20, 2017.
- [25] P. M. Gopal, K. S. Prakash, and S. Jayaraj, "WEDM of Mg/CRT/BN composites: effect of materials and machining parameters," *Materials and Manufacturing Processes*, vol. 33, no. 1, pp. 77–84, 2018.
- [26] K. Anand Babu and R. Jeyapaul, "Process parameters optimization of electrical discharge wire cutting on AA6082/Fly Ash/Al₂O₃ hybrid MMC using taguchi method coupled with hybrid approach," *Journal of the Institution of Engineers*, vol. 102, no. 1, pp. 183–196, 2021.
- [27] R. Krishankumar, H. Garg, K. Arun, A. Saha, K. S. Ravichandran, and S. Kar, "An integrated decision-making COPRAS approach to probabilistic hesitant fuzzy set information," *Complex Intell Syst*, vol. 7, no. 5, pp. 2281–2298, 2021.
- [28] A. R. Mishra, P. Liu, and P. Rani, "COPRAS method based on interval-valued hesitant Fermatean fuzzy sets and its application in selecting desalination technology," *Applied Soft Computing*, vol. 119, Article ID 108570, 2022.